Characterisation of a 30 A Heaterless Hollow Cathode

IEPC-2019-802

Presented at the 36th International Electric Propulsion Conference
University of Vienna • Vienna, Austria
September 15-20, 2019

Alexander J.N. Daykin-Iliopoulos[1] and Igor O. Golosnoy[2] Steve B. Gabriel[3]
University of Southampton, SO17 1BJ, United Kingdom

Franco Bosi[4]
Mars Space Ltd, Southampton, SO14 5FD United Kingdom

Abstract: A novel high-current heaterless hollow cathode (HHC) has been designed, constructed, and tested, with the developed system successfully demonstrating operation up to 30 A. This system overcomes the need for excessive ignition voltages or propellant pulsing, by utilising a reduced keeper orifice that enables ignition with <350 V, and nominal flow rates (<15 sccm). The system has also demonstrated full ignition in 50 seconds compared with conventional ignition, which can require more than 10 minutes; additionally, the system requires as little as 1/6th of the ignition energy compared to that of conventional designs. The HHC's performance was characterised with operation tested in Xe, Kr and Ar. Optical pyrometry has allowed measurements of the emitter tip temperature of a HHC for the first time. Furthermore, the internal cathode-keeper plasma has been investigated using optical emission spectroscopy to determine the plasma electron density.

Nomenclature

A	=	Richardson's constant	S	=	Emitting surface area
e	=	Electron charge	T_t	=	True temperature
I	=	Current	T_i	=	Indicated temperature
J	=	Current density	ζ	=	Optical transmittance
$K_\emptyset$	=	Keeper orifice diameter	λ	=	Wavelength
k_b	=	Boltzmann's constant	$\emptyset_o$	=	Work function

I.Introduction

THE development of high-power hollow cathodes is of importance to meet the demand of increasingly powerful Gridded Ion Engines and Hall Effect Thrusters.[1] Higher power cathodes are increasingly utilizing lanthanum hexaboride (LaB_6) emitters, due to their high-density emission, lifetime and reasonable handling capabilities. However, LaB_6 cathodes theoretically operate at temperatures ~400 K higher than traditionally used Barium Oxide

[1] Electric Propulsion Research Fellow, Tony Davies High Voltage Laboratory, Electrical Power Engineering, Alexander.Daykin-Iliopoulos@soton.ac.uk.
[2] Associate Professor, Tony Davies High Voltage Laboratory, Electrical Power Engineering, ig@ecs.soton.ac.uk.
[3] Professor, Tony Davies High Voltage Laboratory, Electrical Power Engineering, sbg2@soton.ac.uk.
[4] Electric Propulsion Research Engineer, Mars Space Ltd, Franco.Bosi@mars-space.co.uk.

cathodes, which operate around 1500 K. This poses greater challenges for raising the emitter temperature to these higher emissive temperatures in order to enable cathode ignition.

The ohmic heater component, commonly used to raise the emitter temperature to enable thermionic emission, has inherent reliability issues from thermal fatigue caused by the thermal cycling with large temperature variations, further exacerbated with use of LaB_6. A heaterless hollow cathode (HHC), in which the emitter heating is driven by a discharge between the keeper and emitter, allows for potentially higher reliability through design simplicity. There are also multiple other benefits, including reduction in ignition time from minutes to seconds, due to direct emitter heating through ion bombardment, and reduced cost, due to the removal of the heater and the corresponding power supply.

Conventional cathodes have achieved heaterless ignition,[2] though this requires very high ignition voltages (>1 kV) and flow rates (>50 sccm). Therefore, alternative dedicated HHCs are being developed, which have a reduced keeper orifice that increases pressure in the cathode-keeper gap. These devices have demonstrated ignition at nominal flow rates (<15 sccm), with reasonable ignition voltages (<0.5 kV).[3, 4] However, a potential drawback of this configuration is the reduced cathode-anode electron extraction efficiency, ε_{c-a} due to the reduced keeper aperture. This can result in a higher floating keeper voltage for a given current, and likely increased keeper erosion.

This study investigates the influence of the keeper orifice size, $K_{\emptyset}$ on HHC ignition, as well as presenting performance and ignition diagnostic analysis for modelling and design optimisation efforts. This is achieved utilising an instrumented UoS-HHC,[4] which has demonstrated heaterless ignition and operation up to 30 A. The keeper orifice is systematically varied from 0.25 – 1.8 mm, with testing at various discharge currents, 1-30 A. In addition, emitter thermal diagnostics from pyrometer measurements determine pressure and gas species influence on HHC performance. Finally, spectrographic analysis of the keeper-cathode region allows for plasma density measurements.

II.Experimental Setup

A. HHC System

A schematic of the UoS 30 A LaB_6 heaterless hollow cathode is shown in Figure 1. The HHC has been described in a recent paper,[4] so only a brief overview is given here. The heaterless hollow cathode consists of a stainless-steel mounting flange, which attaches to the vacuum chamber mounts via bolts that are electrically isolated with ceramic alumina corner washers. The cathode propellant line protrudes from the rear of the mounting flange, and connects to a 1/8-inch Swagelok fitting, with a ceramic isolator upstream, that is attached to the main propellant line of the chamber. A molybdenum cathode tube 70 mm in length with a 4.9 mm inner diameter is secured to the mounting flange. The lanthanum hexaboride emitter with an inner diameter of 2 mm, outer diameter of 4.5 mm, and a length of 20 mm is inserted into the end of the molybdenum cathode tube. A fine graphite sleeve is used to electrically connect, yet mechanically separate the LaB_6 emitter from the refractory tube, due to the known issues of boron diffusion.[5] A casing supports the multi-layered molybdenum thermal shield wrapped around the cathode tube, which reduces the radiative thermal losses of the HHC during operation.

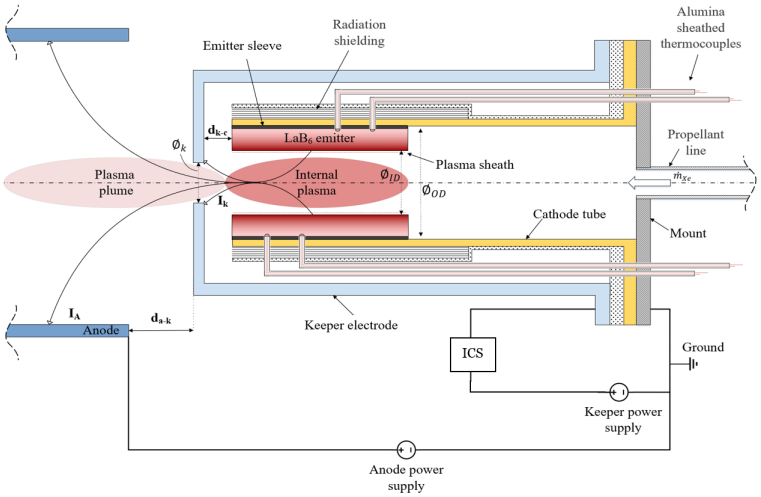

Figure 1: UoS LaB_6 heaterless hollow cathode, with thermocouple instrumentation and simplified electrical scheme.

An overview of the electrical scheme developed for the high current heaterless hollow cathode system can be seen in Figure 2. An EA-PS 9750-12, 750V-12A power supply, applies a potential to the keeper through the ignition control system (ICS), which stabilises the current rise during ignition. The keeper-cathode voltage and current are measured by a Pico Technology TA042 differential voltage probe, that measures up to 1400 V with an accuracy of ±2%, and a LEM Model PR1030 current probe, which can measure up to 1000 A with an accuracy of ±1% read value plus 500 mA. Both probes are connected to a Tektronix DPO3034, 300MHz, 2.5 Gsps Digital Oscilloscope, which displays and records the data. An EA-PS 9200-70, 200V-70A power supply applies the potential to the anode, for igniting and maintaining an anode discharge. The probes, scope, and power supplies are manufacture calibrated. Both the keeper and anode supply negatives are connected to a star ground point. With heaterless ignition, a separate power supply for the heating stage is not required due to the plasma heating the emitter from cold.

The thermocouple instrumentation is connected to a manufacture calibrated Pico Tech TC-08 logger that, along with the power supplies, oscilloscope, MFCs, and pressure gauges, is connected to a PC and logged by a LabView program. The LabView interface allows for both direct operational control and 4 Hz logging of all the applicable equipment. The electrical discharges can cause interference to the PC control system, so all interfaces between the control system and test apparatus are isolated via inline USB/RS232 optocouplers. The electrical system used is the same for the vacuum facilities described in the following sections, except for the anode power supply, which is not used with the keeper discharge facility, as no anode is present in those tests.

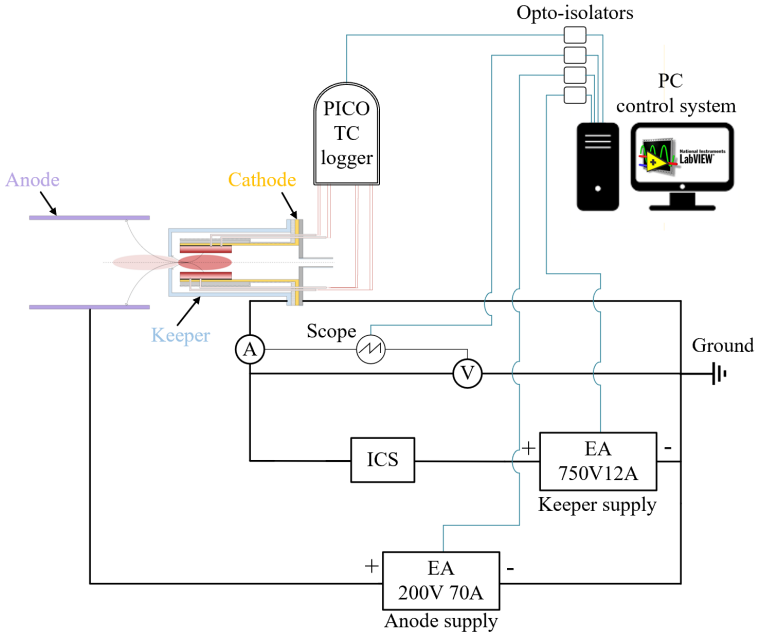

Figure 2: Heaterless hollow cathode electrical scheme.

B. Test facilities

1. Anode Discharge Testing Facility

To test the HHC with gas flow and an anode discharge, TDHVL-VC1 is utilised (see Figure 3). The chamber is 1.2 m long and 0.6 m in diameter with a hinged door for quick access, and a 0.1 m diameter view port at the far end for optical access. The chamber system is roughed and backed by an Edwards E2M80 pump, with two ultra-high throughput Edwards STP-iXA4506C turbomolecular maglev pumps giving a combined 8600 L/s (N_2) pumping speed. The system reaches a base pressure of $<1*10^{-8}$ mbar and maintains a pressure $<5*10^{-5}$ mbar during all the flow tests conducted on the HHC. The low vacuum pressure is measured with an Applied Vacuum calibrated Edwards APG-M Active Pirani Gauge, with an Edwards active gauge controller. The high vacuum pressure is measured with a manufacture calibrated Kurt J. Lesker 354 Series Ion Gauge, with pre-configured correction factors for the gases used.

The VC1 door has a mounting plate on the inside, which the HHC attaches to. In addition, there are four NW40CF as well as one NW16CF ports on the door for various electrical and gas feedthroughs. The cathode is electrically connected to the mounting plate, which is grounded. The mounting plate in turn is connected to the door via support rail. The anode is also mounted to the support rail system, with slots in the rail system allowing the separation between anode and keeper downstream orifice to be varied (d_{k-a}). This is nominally set to 10 mm. Both the cathode mounting plate and anode are supported with Macor stand-offs from the support rail to provide electrical and thermal insulation.

Around 1.5 m upstream from the HHC a manufacture calibrated Applied Vacuum Barometric 0.5-25 mbar dial gauge measures the propellant line pressure, with an accuracy of ± 0.25 mbar. Upstream from the dial gauge a manufacture calibrated Bronkhorst EL-FLOW mass flow controller (MFC) sets the HHC flow rate, with a 0-20 sccm range and an accuracy of ±0.5% read value plus ±0.1% full scale value, such that the maximum error (at 20 sccm) is ±0.12 sccm. The MFC is connected to the regulator of the corresponding noble gas cylinder used for the experiment. The following gases and corresponding purities were utilised for the HHC testing presented in this paper: Ar (N5), $ArH_2$1% (N5), Kr (N5), $KrH_2$1% (N5), and Xe (N4.8), where N5 is 99.999% and N4.8 is 99.998% pure. This purity is sufficient given that the emitter employed is LaB_6 and not BaO-W. 1/4 and 1/8 inch Swagelok fittings are use throughout the propellant line system and are leak tested prior to operation.

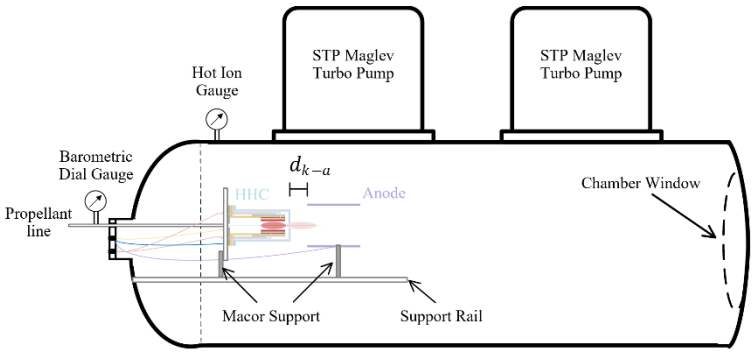

Figure 3: TDHVL - VC1 vacuum facility, with the HHC anode discharge configuration.

2. Keeper Discharge Testing Facility

TDHVL - VC3 vacuum facility (see Figure 4) was utilized for testing due to the backfilling capability. The facility consists of a 35 cm diameter spherical stainless-steel vacuum chamber, with numerous CF16, CF40 & CF100 flanges, allowing for easy instrumentation access and mounting. An Edwards RV5 vacuum pump reduces the chamber base pressure to ~$9*10^{-3}$ mbar at which point an Edwards Next 400D turbo pump controlled via the PC interface, lowers and maintains a base pressure of <$1*10^{-6}$ mbar prior to operation. A gate valve is connected between the turbo pump and the vacuum chamber to allow isolation of the turbo pump, so that backfilling is possible. The chamber pressure was measured by a Pfeiffer Balzers IKR-020 Penning gauge and a TPR 010 Pirani gauge, displayed on a TPG-300 vacuum gauge controller, correction factors are implemented for the operating gas, though the inaccuracy beyond 0.5 mbar for noble gases is too great to measure the backfilled pressures, >0.5 mbar. Thus, the Barometric 0.5-25 mbar dial gauge was utilised to determine the backfilled pressure as well as the propellant line pressure when flow is used.

The system backfilling is conducted by reducing the pressure to <$5*10^{-8}$ mbar, to remove gas impurities from the system. Then the chamber isolation valve is closed, and the pressure is rapidly raised by utilising a bypass valve, such that within ~5 seconds the whole chamber reaches close to the required pressure (typically 2-10 mbar) and further fine pressure adjustment is conducted by the prior discussed MFC propellant system.

The VC3 HHC backfilled configuration (shown in Figure 4, left diagram) is where the keeper from the HHC (see Figure 1) is removed, and an open keeper is placed downstream of the cathode, with the system backfilled as described. The chamber window allows for direct pyrometer measurements of the HHC emitter and analysis of optical emission from the cathode-keeper discharge, through a fibre mounted on the window. Additionally, keeper discharge flow tests are conducted in VC3 (shown in Figure 4, right diagram). In such tests, the HHC is operated with the original enclosed keeper attached with the flow injected through the cathode propellant line and the system is not backfilled. In both these VC3 configurations, no anode is utilised.

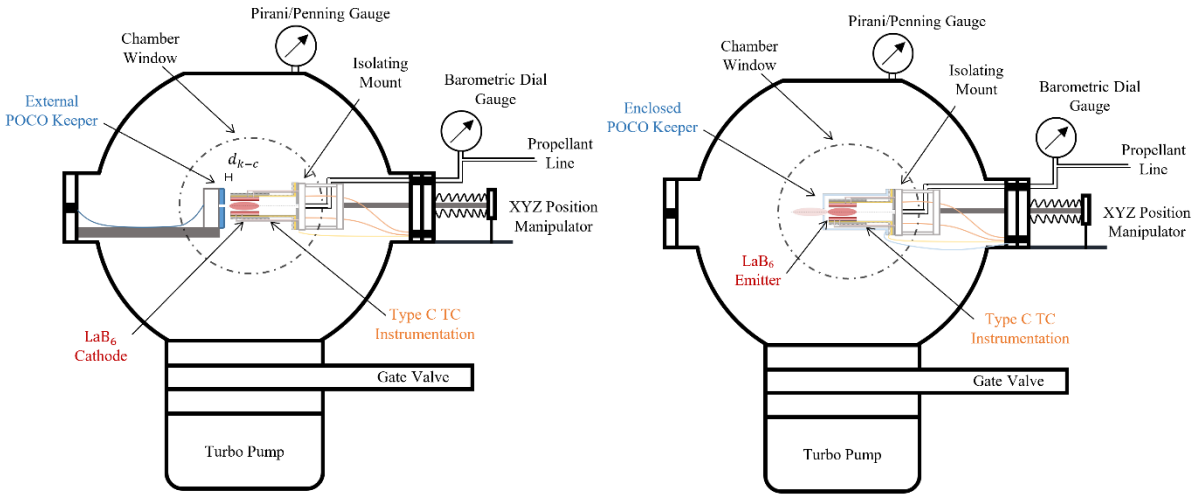

Figure 4: TDHVL - VC3 vacuum facility, HHC configuration with a backfilled open keeper (shown left), and enclosed keeper with flow (shown right).

C. Diagnostics

1. Pyrometer Measurements

The backfilled open keeper configuration allows direct optical access of the emitter surface, thus allowing optical thermal measurements of the emitter (see Figure 1 & Figure 4). Optical access is viable with a keeper-emitter separation ≥2 mm, with the emitter downstream annular surface and central hole edge being visible. The upstream view of the inner-hollow emitter surface was very limited by the viewing angle and keeper obstruction. Measurements are taken on the annular surface, to avoid interference from the plasma radiation, which is strongest in the central hollow emitter region, though typically the measurement difference across the whole viewed emitter surface was less than 50 °C.

These measurements are conducted with a manufacturer calibrated Spectrodyne Inc. DFP 2000 portable disappearing filament optical pyrometer. This pyrometer operates at a wavelength, λ, of 0.65 μm, and has a total range of 760 °C to 4200 °C. The pyrometer range operated in these experiments maintained an accuracy of 0.3% of the measurement reading ±1 °C. For accurate pyrometer measurements corrections are required for the emissivity, ε, of the target at the measured wavelength. In addition, adjustment to the emissivity is required to take account of the chamber window optical transmittance, ζ, at λ, such that the effective emissivity [6] $\varepsilon_{\lambda_{e,\zeta}} = \varepsilon_\lambda \, \zeta_\lambda$. For the borosilicate glass window of the chamber the optical transmittance is taken to be $\zeta_\lambda = 0.91$ and the LaB_6 emissivity [7] is:

$$\varepsilon_\lambda = 1.2144 - 2.467 * 10^{-4} T_i \tag{1}$$

so to correct from the indicated temperature, T_i, in K, measured by the pyrometer at $\lambda = 650$ μm to the true surface temperature [8] T_t in K:

$$T_t = \frac{1}{\left(\frac{1}{T_i}\right) + \left(\frac{log\ \varepsilon_{\lambda_{e,\zeta}}}{9613}\right)} \tag{2}$$

2. Spectrographic Plasma Analysis

Optical emission spectrographic analysis of the hollow cathode discharge is conducted to determine the plasma electron number density in the backfilled configuration (see Figure 4, left diagram). The optical system consists of a FG200AEA, 200 um, 0.22 NA, optical fibre, which is mounted to the chamber window. This fibre mounting gives a

line of sight over the emitter-keeper discharge, such that the electron density measured is an average over the length and cross-section of the emitter-keeper discharge. During the plasma density measurements, the emitter-keeper separation was set to 4 mm, and the discharge cross-section is not contained due to the open keeper used in the backfilled configuration. The fibre connects to a Princeton Instruments SP-2750, 0.750-meter focal length, triple grating imaging spectrograph, with a PI-MAX 3 1024i ICCD camera. The highest resolution grating of 2400 gr/mm was used for these experiments. The system is wavelength and intensity calibrated by an Ocean Optics HG-1 mercury-argon source and an Ocean Optics DH-3P-CAL deuterium-tungsten source respectively. The spectrograph is operated with PI WinSpec software. A gain of 100 was used for the data gathering combined with a gate width of 0.5 to 2 seconds. Each spectrum taken was a set of 10 accumulations, which increases signal to noise ratio, and each plasma density measurement is a mean of at least 4 spectra sets.

The plasma electron density is estimated via Stark broadening of hydrogen Balmer lines, using procedure outlined by Konjević.[9] This links the fitted Voight profiles of the $\lambda_{\mathrm{H}-\beta}$ line at 486.135 nm to the plasma electron density. The fitting was done utilising a processing script which accounts for neighbouring line verified within Horizon2020 PATH project.[10, 11] To enable $\lambda_{\mathrm{H}-\beta}$ broadening measurements the HHC was operated with 1% H_2 for argon and krypton, such that the gas mixtures used were Ar$H_2$1% and Kr$H_2$1%. The addition of 1-3% H_2 is typically employed for such measurements,[9, 12] in order to attain a measurable intensity of the $\lambda_{\mathrm{H}-\beta}$ line to enable calculation of the plasma density with minimal interference to the plasma properties, as non-negligible collisional quenching of Ar excited states and ions start at mixtures above 15%.[13] Attempts for plasma electron density measurements with Xe, with mixtures of 1-10% H_2, proved unsuccessful due to intense Xe emissions concealing the H-β line. The H-β line broadening under plasma conditions such as those found within in-space cathodes with electron densities typically around $1{*}10^{19}$ - $1{*}10^{21}$ m^{-3} and electron temperatures around 1-3 eV are affected by the following broadening mechanisms:

- Stark broadening, in which the emitter's natural emission frequency is altered by the plasma's local electric field and is hence sensitive to changes in plasma density. This effect is characterised approximately by the Voigt profile at low plasma densities.
- Doppler broadening, from the thermal motion of the emitter changing the observed emission frequency, and as such sensitive to the gas temperature. This effect is characterized by a Gaussian profile shape.
- Instrumental broadening related to the spectrometer optical system, which is characterized by a Gaussian profile shape.

The instrumental function of the spectrometer is a Gaussian profile with a wavelength dependent full width at half maximum (FWHM), $w_I(\lambda)$. Utilising the wavelength calibration source, for this optical system w_I, at a wavelength λ, in nm, was found to be

$$w_I(\lambda) = 0.049 - 3.7 * 10^{-5} \cdot \lambda \tag{3}$$

A Voigt profile fit is applied to the H-β experimental profile, which was found by Konjević to provide a suitable approximation. Though as seen in the data (see Figure 5), for this plasma a single ionised lanthanum line at 486.091 nm overlays the H-β line at 486.135 nm. Thus, an additional Gaussian fit is required to be applied to the La II line, and then convoluted to the formed H-β fit to confirm the overall fit. The final convoluted fit can be seen to have good agreement with the experimental data, as shown in Figure 5. The formed H-β fit is correlated to the electron density, n_e, in m^{-3} by [9]

$$n_e = 10^{22} * (0.94666 * w_s)^{1.49} \tag{4}$$

where w_s in nm is the H-β FWHM given by

$$w_s = \left(w_V^{1.4} - w_{D,I}^{1.4}\right)^{1/14} \tag{5}$$

and where w_V is the Voigt profile FWHM, (see Figure 5), $w_{D,I}$ is the FWHM of the Gaussian resulting from convolution of doppler, w_D, and instrumental broadening, w_I, profiles and given by

$$w_{DI} = (w_D^2 + w_I^2)^{0.5} \tag{6}$$

Finally, the doppler broadening, w_D, is given by [14]

$$w_D = \lambda_{H-\beta} \left(8ln\ 2 \frac{k_b T_g}{M_a c^2} \right)^{0.5} \tag{7}$$

where k_b is the Boltzmann constant in $m^2\ kg\ s^{-2}\ K^{-1}$, M_a is the mass of the H-β emitter, $1.66 * 10^{-27}$ Kg, c is the speed of light and T_g is the gas temperature in K, taken to be from 2000-8000 K, as shown in Figure 5. It can be seen the gas temperature uncertainty has a relatively small influence on the electron density estimation. In addition to this, there is good repeatability between measurement sets.

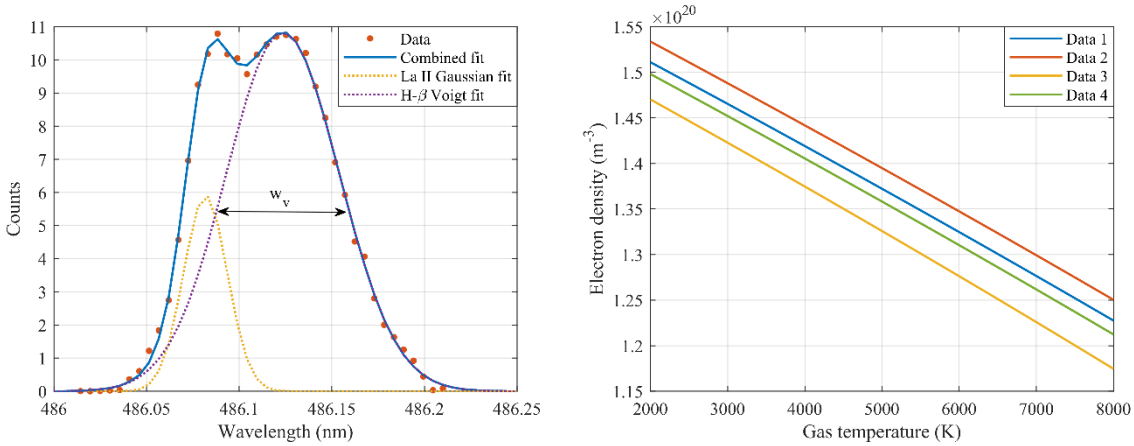

Figure 5: Backfilled open keeper configuration with a 1 A, 5.5 mbar (Ar) discharge, example spectra profile fitting (shown left) and electron density as a function of gas temperature (shown right).

III.Results and Discussion

A. Anode *V-I* Characteristics

Once a cathode is ignited with a nominal keeper discharge, the discharge is then transferred to the thruster discharge chamber or ion beam for main operation. Alternatively, the discharge can be transferred to an anode to simulate operation with the thruster, which can also give a stable benchmark for cathode testing. However, unfortunately, there is still no standardisation within the EP field on anode test configurations, and therefore comparisons between different cathodes are challenging. The HHC has been tested in the anode discharge test facility, see Figure 3. The HHC is tested with a keeper aperture of 1.8 mm. To ignite the HHC, 13 sccm xenon was injected through the propellant line, the keeper power supply was set to 1-2 A, and 700 V, and applied. This creates a keeper discharge which heats the emitter from ~20 °C to thermionic emission temperatures within a minute.

Once the HHC was ignited and thermionically emitting with the keeper discharge between 1-2 A, the discharge is maintained for a stabilisation period of 1-3 minutes then the anode potential is applied, with the anode current limited initially to 0.5 A and then levelled up to the required setpoints. This gradual ramp-up is to support the discharge

stability. Once the anode discharge is beyond 1 A, the keeper discharge is switched off, such that the keeper is left floating, which is a typical practice for most conventional discharge HCs.

Throughout ignition of the HHC for the anode discharge tests, the xenon mass flow rate was set to 13 sccm. The HHC anode discharge *V-I* characteristic from 1-30 A is shown in Figure 6. The discharge voltage is initially significantly higher, with 60 V at 1 A, halving to around 30 V at 5 A, this effect is merely to sustain the discharge power for sufficient heating of the emitter via ion bombardment. With increasing current from 5 to 20 A the discharge voltage can be seen to level off, around 20 V, with little change above 10 A, this is typical of hollow cathodes.[15] Though with further increases in discharge current HCs have a small variance in the discharge voltage until the current becomes too high and the voltage begins to rise.[15] The discharge voltage rise at high current is typically due to the thermal balance of the cathode, with increasing radiative losses at higher temperature operation, requiring increased ion bombardment. The thermal design of the cathode can significantly influence the magnitude of this trend, due to the thermal balance.

The HHC was sized for a nominal discharge current of 20 A, though due to research aims of high power HHC development, this HHC was operated up to 30 A, as shown in Figure 6 and Figure 7. During this high current anode testing, operating at >20 A, no adverse effects, such as a rise in discharge voltage mentioned, high voltage fluctuations or shifting to plume mode were detected. Thus, this indicates that the HHC is stable at 30 A and could perhaps operate at higher current, though higher current operation was not tested precautionarily. If the HHC were to operate at very high currents, beyond 50 A, the discharge voltage would likely rise as discussed and given the sizing of the cathode such operation would significantly reduce HHC lifetime, hence, re-sizing would be required for such operation

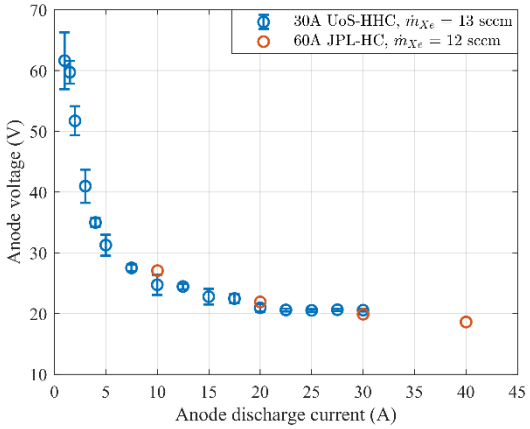

Figure 6: Anode discharge V-I characteristics for the UoS-HHC and JPL-HC[1].

The performance of a well-established conventionally heated LaB_6 HC from JPL NASA[1] is also displayed in Figure 6. It must be noted that direct quantitative comparison of the HHC and the JPL HC would be misleading due to a lack of standardised cathode testing as discussed, leading to inevitable variance in test conditions. Specifically, it is well known that the anode geometry and positioning have a strong impact on performance. Furthermore, the conventional JPL cathode displayed is designed for current operation 3 times higher than the HHC and operates with a magnetic field that can raise the voltage by 2-3 V.[1, 16] Hence this plot does not discern in any way which cathode has better performance. Nevertheless, the striking similarity in operational trends is a good initial indication that this heaterless ignition method does not significantly degrade nominal operational performance of the HHC, while achieving the fast heaterless ignition with nominal flow rates.

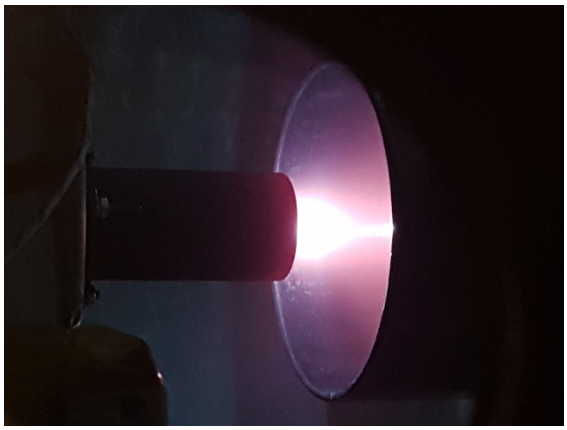

Figure 7: UoS-HHC 30 A anode discharge with 13 sccm (Xe)

B. Keeper Orifice Influence

As discussed, the keeper orifice is reduced in comparison to conventional HCs for the purpose of increasing the emitter-keeper pressure to induce sub-kilovolt breakdown. However, the keeper orifice size influences the current extraction to the anode as shown in Figure 8. For a keeper orifice diameter of 0.25 to 1.8 mm the maximum keeper orifice current density extraction to the anode was recorded. For the 0.25 and 0.4 mm keeper orifice the anode supply was set to the maximum potential of 200 V. At 1 mm diameter the discharge voltage was increased to a maximum of 73 V, and the current extracted was 7 A, and although potentially higher current could be extracted to the anode by increasing the voltage further, this was avoided due to the discharge becoming highly volatile, effectively limiting current density extraction below 800 A/cm^2 for the 1 mm keeper orifice. For the 1.8 mm orifice, the current extraction was not found to be limited up to 30 A, as was shown in Figure 6, and thus could potentially reach significantly higher extracted current densities with that orifice size. The mass flow rate for each orifice size was adjusted to maintain a minimum flow rate while still in spot mode operation, this was between 1-13 sccm Xe throughout these tests.

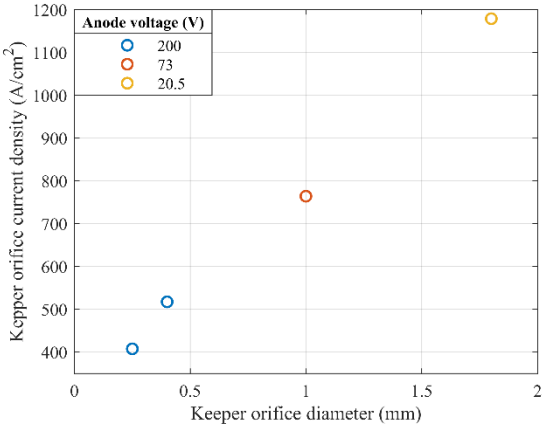

Figure 8: Maximum current density extracted through the HHC keeper orifice for various keeper orifice diameters.

Although this data inevitably has more than one varied parameter, it still clearly shows that the maximum extracted current density increases significantly with orifice size. For a 62.5% increase in orifice diameter the extracted current density increases by 75%, this enhancement is perhaps due to reduced wall losses, from the enhanced electron extraction from the emitter to the anode with the less constrictive orifice, such that the current density increases.

C. Keeper Floating Voltage

The floating keeper potential is shown in Figure 9, again with the JPL-HC for reference, with the prior mentioned caveats when quantitively comparing. The keeper floats positive by around 55 V at 1 A with high variance, then drops rapidly within the first 5 A, before levelling off, with a very similar profile to that of the discharge voltage. The trend beyond 5 A is similar to that of the conventional JPL cathode, though the magnitude is significantly higher. The JPL keeper orifice is 68% larger than the emitter ID,[5] whereas the HHC keeper in this configuration is about 6% smaller than the emitter ID, such that it constricts the plasma flow, effectively like a conventional orifice as mentioned. As the HHC keeper has a smaller orifice compared with conventional HCs, it collects more charged particles. The floating condition balances the ion and electron fluxes to have a zero-net current, such that the higher keeper floating voltage indicates increased ion bombardment to the keeper. Though the keeper erosion will significantly depend on the keeper-plasma potential difference, due to the non-linear sputter yields.[17, 18]

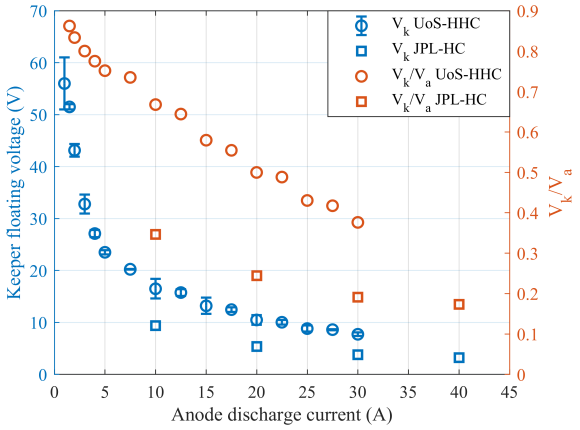

Figure 9: Floating keeper *V-I* characteristics for the UoS-HHC and JPL-HC[1] in anode discharge mode.

Interestingly it can be seen in Figure 9 that the HHC keeper floating voltage, V_k, as a proportion of the anode discharge voltage, V_a, decreases almost linearly from 0.88 at 1 A to 0.38 at 30 A. The keeper floating measurement shows that as the discharge current increases, V_k drops at an increased rate, this is perhaps due to the thermionic emission proportion of the current increasing with increased discharge current, thus changing the net charge balance in the keeper potential. The conventional JPL cathode also shows V_k reducing at an increased rate to V_a, though as a much smaller proportion of the discharge current, from 0.35 at 10 A to 0.19 at 40 A.

D. Gas Species Influence

The emitter downstream end was measured with an optical pyrometer, as described in Section II.C, from the transition to thermionic emission which occurs around 0.3 A to nominal keeper discharge operation above 1 A. The pyrometer gives accurate temperature measurements of the emitter tip through this process, however below 0.3 A the thermal radiation emission is too low for the pyrometer to accurately measure, hence measurements begin from 0.3 A. Figure 10 displays the emitter tip temperature and *V-I* characteristics for Ar, Kr and Xe gases in the backfilled open keeper configuration, see Section 2, at 5.5 mbar with a 4 mm cathode-keeper separation.

Figure 10 shows that the emitter tip temperature increases steeply from 0.3 to 0.5 A, going from around 1100 ℃ for all three gases and increasing by 125 ℃ for Xe, 225 ℃ for Kr and 275 ℃ for Ar. Beyond this, the emitter temperature increases are significantly smaller, as the discharge is more significantly thermionically emitting. The voltage can be seen to drop significantly during this process as expected. The higher voltage and temperature of the emitter for argon is likely due to the higher ionisation potential, and lower ion mass, requiring a higher electric field strength to maintain sufficient ionisation, which also increase the ion bombardment energy to the surface, thus increase the emitter temperature and therefore the thermionic emission. Additionally, at 0.3 A the temperature difference between the gas species is the smallest, indicating a higher proportion of secondary emission discharge at this stage compared to that of the 0.5 A. These results support that the transition period occurs in which the discharge is both a

thermionically and secondary emission sustained discharge. This stage is found to be stable, via power supply current limitation, for only short periods of time, typically <5 minutes, as either it will switch to a thermionic regime, or cathode spots can appear, in which damaging discharge localization occurs. Thus quick, though stable transfer through this transition period is critical for successful HHC ignition.

Figure 10 also plots the predicted thermionic emission, where the current density J, in $\mathrm{A/cm^2}$, produced from thermionic emission of a material is predicted by the Richardson–Laue–Dushman equation[19, 20]:

$$J = AT^2 e^{-\frac{e\emptyset_o}{k_b T}}, \tag{8}$$

where T is temperature in K, $\emptyset_o$ is the classical work function, e is electron charge, k_b is Boltzmann's constant, and A is the Richardson's constant, ideally $120 \frac{\mathrm{A}}{\mathrm{cm^2}}\ \mathrm{K^2}$. The Richardson equation allows for calculating the emitter temperature required to provide the current from thermionic emission only, with $J = I/S$, where S is the exposed emitter surface and I is the discharge current. As such the Richardson equation is plotted for varying surface attachment, from 30% to 100% of the emitter surface. The thermionic profile matches the Ar plot from 0.5 to 1.3 A, for a $0.6S$ well. Though the HHC thermal profile shows a large temperature gradient from T_4 to T_1 in nominal operation,[21] indicating that less than 50% of the emitter is active. Hence there is a disparity in the predicted and measured tip temperature. Other groups have also reported lower temperatures than predicted for LaB_6,[22] which may be due to lanthanum recycling mechanisms converting the LaB_6 to LaB_4 which has a lower work function. Though alternatively, this disparity may be due to a sizable ionic current, thus requiring less thermionic emission to sustain a given current. The trend agreement between the experimental and predicted emission supports that from 0.5 A the discharge current increases are supplied by predominately thermionic emission.

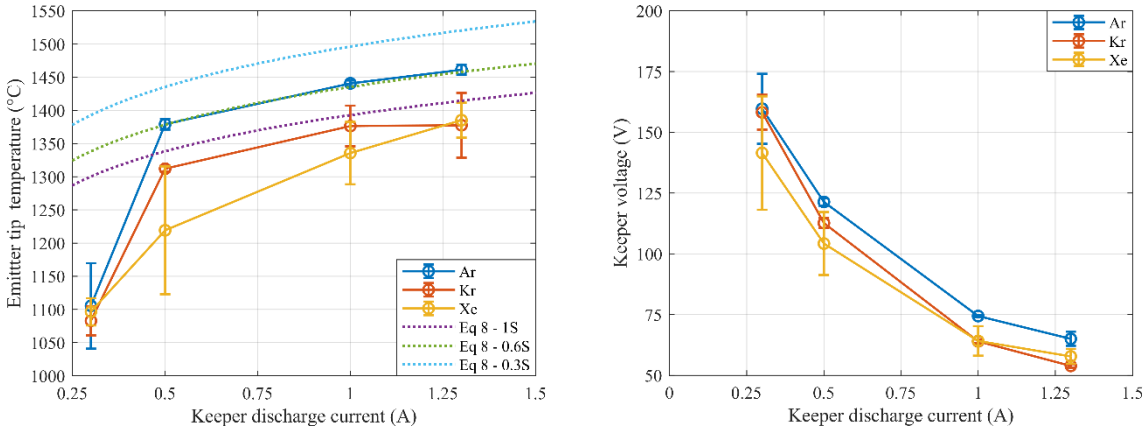

Figure 10: Influence of gas species on emitter tip temperature and keeper voltage in the backfilled open keeper configuration, 5.5 mbar, 4 mm separation.

E. Pressure Influence

The pressure influences on the transition to nominal keeper discharge were investigated in the same backfilled open keeper configuration with pyrometer measurements as with the prior section on the gas species investigation. Although only Xenon is used for the pressure investigation. Three keeper discharge pressures, 2, 5.5 and 10 mbar are shown characterised in Figure 11. These operating pressures are stable and repeatable once the HHC is ignited to the transition or nominal operation phase. The HHC cannot breakdown and form a stable secondary electron emission sustained discharge with pressures below ~4 mbar and above ~7 mbar, due to the discharge not attaching uniformly or at all to the emitter outside this pressure range. 5.5 mbar was empirically found to consistently operate across Ar, Xe and Kr to efficiently ignite the discharge, hence this was defined as a standard setpoint for various tests. Thus, to conduct these pressure influence tests the ignition was achieved with a pressure first set to 5.5 mbar, and then once

ignited to a keeper current of 1 A, the pressure was adjusted to the required value and the current was varied from 0.3 to 1.3 A.

The pressure influence on the keeper discharge is apparent in the tests shown in Figure 11. From 10 mbar to 2 mbar there is a ~20% increase in keeper discharge voltage across the current range which corresponds to a nearly 15% increase in emitter tip temperature at 0.3 A, that gradually drops to a 2.5% increase at 1.3 A. This indicates that at lower pressure the increase in the ionisation mean free path, results in an increase in the voltage to sustain the required ionisation incidents. The increase in voltage also increases the energy of the ion bombardment, further heating the surface. The 15% temperature increase from 10 mbar to 2 mbar at 0.3 A indicates that the thermionic emission component of the discharge current increased as pressure decreased due to the reduction in the ionisation incidents. As the current rises the thermal differences between the three pressures measured reduces, this is perhaps partially due to the discharge changing to a mostly thermionic discharge at this current level, and hence reducing the dependency on gas pressure. Also, at higher temperatures the thermionic emission sensitivity increases, such that small temperature differences gives rise to large emission current differences. The 2 mbar pressure sustains higher voltage than the 5.5 and 10 mbar pressures despite the emitter temperature difference reducing, this is still likely due to the increase in the ionisation mean free path, so that the higher voltage is required to attain the equivalent emitter heat flux. Finally, the Richardson curves show the same effect as seen for the gas species plots, with the measured temperatures significantly below that of the prediction, given plausible surface attachment assumptions, as discussed.

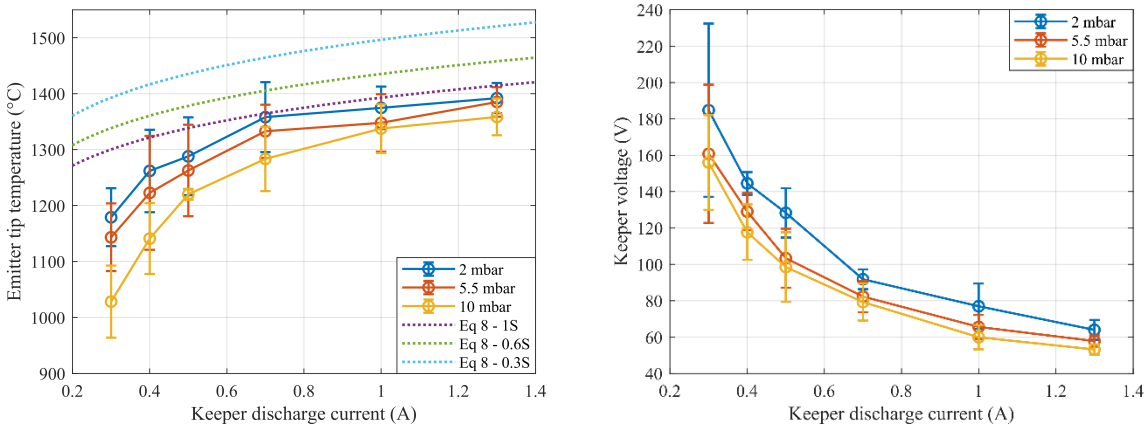

Figure 11: Influence of pressure on the emitter tip temperature and keeper voltage in the backfilled open keeper configuration, Xe, 4 mm separation.

F. Plasma Density Characteristics

The cathode-keeper plasma electron density, n_e, for Kr and Ar is measured spectrographically in the backfilled open keeper configuration, with the procedure and setup outlined in Section II.C. As discussed, the Xe discharge electron density was unable to be measured with this approach due to a relatively strong Xe ion line concealing the $\lambda_{\mathrm{H}-\beta}$ line. The results of the plasma electron density verses keeper discharge current are shown in Figure 12. The Kr mean density is initially around $2.4{*}10^{20}$ m^{-3} compared with $1{*}10^{20}$ m^{-3} for Ar at a keeper current of 0.4 A. $\bar{n}_{e,Kr}$ can be seen to rise initially at 0.5 A and then gradually decrease up to 2 A. $\bar{n}_{e,Ar}$ appears to have a similar trend of increasing up to 1 A, and with the mean then decreasing at 1.3 A. Though considering the error in the measurement the actual density could be almost constant. The cause of the electron density being static, or decreasing is likely a result of the measurement collecting emission from the whole discharge cross section from cathode to keeper, thus, measuring the effective average electron density of the discharge. It is suggestive that the plasma discharge volume increases due to the unconfined nature of the backfilled open keeper discharge. An increase in discharge volume can cause the average N_e density to decrease, with the core plasma density increasing with current as expected.

The order of magnitude of these plasma density measurements are reasonably close to those of a conventionally heated LaB_6 cathode conducted with Langmuir probes.[5] These Langmuir probe measurements were conducted on a HC with an anode discharge and operated at significantly higher currents, 20-100 A, though the results showed the peak plasma density consistently remaining within ~$5{*}10^{20}$ to $1{*}10^{21}$ m^{-3} for this large current range. Thus, as this

HHC plasma density profile is approximately within an order of magnitude of these results shows reasonable alignment of the data with that available in the literature for comparative LaB_6 systems.

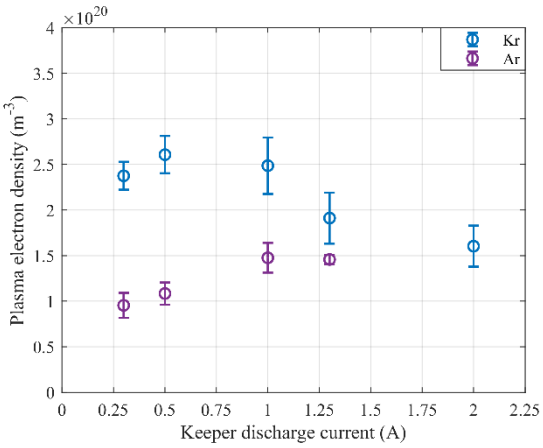

Figure 12: Plasma density characteristics for Kr and Ar in the backfilled open keeper configuration, 5.5 mbar, 4 mm separation.

IV.Conclusion

A novel high current heaterless hollow cathode concept has been developed, constructed and successfully undergone proof of concept and operational characterisation. This operational HHC can ignite with nominal flow rates, below 15 sccm, and does not require any additional propellant pulsing or bypass, in addition the system achieves ignition with voltages below 400 V, with discharge operation demonstrated up to 30 A.

This HHC has been tested in both a backfilled configuration, which allows increased diagnostic access to the system, and a nominal flow configuration, with an anode to simulate in-thruster operation. Diagnostics including direct pyrometer measurements of an emitter surface in a LaB_6 cathode developed for in-space applications and spectrographic electron density measurements of the emitter-keeper gap have been conducted.

Despite the differences with this HHC design configuration to that of conventional HCs, the HHC has demonstrated very similar V-I performance trends from 10-30 A to that of these conventional HCs, which gives an initial indication that the heaterless design modifications does not significantly impact performance. Furthermore, the similar plasma parameters may suggest that the emitter lifetime predictions can be based on the existing models for conventional HCs.

Thus, this developed UoS-HHC is a significant step towards the obsoletion of the conventional cathode heater component. The cathode heater component is a prominent failure mechanism of HCs within electric propulsion systems and is mitigated in the HHC, while also gaining savings in; mass, volume, PPU simplicity, ignition power, and cost.

Acknowledgments

The authors would like to express their gratitude to the Tony Davis High Voltage Laboratory (TDHVL) for their assistance in the fabrication of the heaterless hollow cathode. This work has been conducted in part under a UK Space Agency NSTP Fast Track Project Scheme (Grant agreement ID: NSTP3-FT2-073) and in part under an EPSRC PhD scholarship. In addition, the authors received support from the H2020 PATH project (Grant agreement ID: 734629).

References

[1]E. Chu and D. M. Goebel, "High-Current Lanthanum Hexaboride Hollow Cathode for 10-to-50-Kw Hall Thrusters," *Ieee Transactions On Plasma Science,* vol. 40, no. 9, 2012.

[2]M. Schatz, "Heaterless Ignition of Inert Gas Ion Thruster Hollow Cathodes," in *18th International Electric Propulsion Conference*, Alexandria, USA, September 30-October 2, 1985.

[3]D. Lev, G. Alon, L. Appel, O. Seeman, and Y. Hadas, "Low Current Heaterless Hollow Cathode Development Overview," in *35th International Electric Propulsion Conference*, Atlanta, USA, 2017.

[4]A. J. N. Daykin-Iliopoulos, I. O. Golosnoy, and S. B. Gabriel, "Development of High Current Heaterless Hollow Cathode," presented at the Space Propulsion 2018, Seville, Spain, 14-18 May 2018, 2018.

[5]D. Goebel and E. Chu, "High-Current Lanthanum Hexaboride Hollow Cathode for High-Power Hall Thrusters," *Journal of Propulsion and Power,* vol. 30, no. 1, pp. 35-40, 2014.

[6]K.-D. Gruner, "Principles of Non-Contact Temperature Measurement," Raytek GmbH2003.

[7]E. K. Storms, "The Emissivity of Lab6 at 650 Nm," vol. 50, no. 6, pp. 4450-4450, 1979.

[8]L. Michalski, *Temperature Measurement*. Chicago: Wiley, 2001.

[9]N. Konjević, M. Ivković, and N. Sakan, "Hydrogen Balmer Lines for Low Electron Number Density Plasma Diagnostics," *Spectrochimica Acta Part B: Atomic Spectroscopy,* vol. 76, pp. 16-26, 2012/10/01/ 2012.

[10]UoS, MSL, ALMA, and T4I, "Plasma Antenna Technologies," ed. UK, Italy, Greece: EU Horizon 2020, 2017-2020.

[11]A. J. N. Daykin-Iliopoulos, F. Bosi, T. Papadimopoulos, P. Decarlo, I. Golosnoy, and S. Gabriel, "Characterisation of a Hollow Cathode Apparatus for High-Density Plasma Antenna Applications," *Plasma Sources Science and Technology [In preparation for submission],* 2019.

[12]J. M. Palomares *et al.*, "Hβ Stark Broadening in Cold Plasmas with Low Electron Densities Calibrated with Thomson Scattering," *Spectrochimica Acta Part B: Atomic Spectroscopy,* vol. 73, pp. 39-47, 2012/07/01/ 2012.

[13]S. Siepa, S. Danko, T. V. Tsankov, T. Mussenbrock, and U. Czarnetzki, "On the Oes Line-Ratio Technique in Argon and Argon-Containing Plasmas," *Journal of Physics D: Applied Physics,* vol. 47, no. 44, p. 445201, 2014/10/09 2014.

[14]H.-J. Kunze, *Introduction to Plasma Spectroscopy*, 1 ed. (no. 56). Springer-Verlag Berlin Heidelberg, 2009, p. 242.

[15]D. Goebel, R. Watkins, and K. Jameson, "Lab6 Hollow Cathodes for Ion and Hall Thrusters," *Journal of Propulsion and Power,* vol. 23, no. 3, pp. 552-558, 2007.

[16]D. Goebel, K. Jameson, and I. Mikellades, "Plasma Characterization with Miniature Fast-Scanning Probes," *Journal of Applied Physics,* vol. 98, no. 10, p. 113302, 2005.

[17]R. P. Doerner, D. G. Whyte, and D. M. Goebel, "Sputtering Yield Measurements During Low Energy Xenon Plasma Bombardment," vol. 93, no. 9, pp. 5816-5823, 2003.

[18]R. P. Doerner, "Low-Energy Sputtering Yields of Tungsten and Tantalum," vol. 23, no. 6, pp. 1545-1547, 2005.

[19]O. Richardson, "Electron Theory of Matter," *Cambridge Physical Series,* vol. 23, pp. 594-627, 1914.

[20]K. L. Jensen, *Introduction to the Physics of Electron Emission*. Wiley, 2017.

[21]A. J. N. Daykin-Iliopoulos, I. O. Golosnoy, and S. B. Gabriel, "Thermal Profile of a Lanthanum Hexaboride Heaterless Hollow Cathode," in *35th International Electric Propulsion Conference*, Atlanta, USA, 2017.

[22]J. Polk, D. Goebel, and P. Guerreo, "Thermal Characteristics of a Lanthanum Hexaboride Hollow Cathode," in *International Electric Propulsion Conference*, Kobe, Japan, 2015.